

Original paper

New type of epithermal manganese mineralization from the Banská Hodruša precious and base metal deposit at the Rozália mine, Hodruša-Hámre, Slovakia

Matej RYBÁRIK^{1*}, Martin ŠTEVKO^{2,3}, Peter KODĚRA¹, Ján PRCÚCH⁴

¹ Department of Mineralogy, Petrology and Economic Geology, Faculty of Natural Sciences, Comenius University, Ilkovičova 6, 842 15 Bratislava, Slovak Republic; rybarik9@uniba.sk

² Earth Science Institute, Slovak Academy of Sciences, Dúbravská cesta 9, 840 05 Bratislava, Slovak Republic

³ Department of Mineralogy and Petrology, National Museum, Cirkusová 1740, 193 00 Prague 9, Czech Republic

⁴ Slovenská banská spol., s.r.o., 966 61 Hodruša-Hámre 388, Slovak Republic

* Corresponding author



The newly discovered unusual epithermal manganese mineralization was found at the 18th level of the Rozália mine in the Štiavnica stratovolcano and it is hosted by a NE-SW oriented fault dipping 55° to SE. Based on its structural setting and cross-cut relationship to a pre-caldera vein it belongs to a large system of post-caldera veins related to horst uplift in the central zone of the stratovolcano. The vein occurs in andesite and consists of two contrasting parts, including a part dominated by white coarse-grained calcite and Mn-rich part represented by abundant johannsenite, younger rhodonite and Mn-carbonates (rhodochrosite, Mn-calcite), in association with minor quartz, calcite, adularia, chlorite, and clinzoisite. Ore minerals are represented by sphalerite, galena, pyrite, chalcopyrite and rare inclusions of acanthite and can be found exclusively in the Mn-rich part of the vein. Johannsenite forms greenish-blue, greenish-brown or brown radial aggregates reaching up to 7 cm in size. Its average empirical formula is $\text{Ca}_{0.96}(\text{Mn}_{0.97}\text{Mg}_{0.07}\text{Fe}_{0.03})_{1.07}(\text{Si}_{1.98}\text{Al}_{0.02})_{2.00}\text{O}_6$. Rhodonite shows a significant compositional variation of Ca and Mn contents, ranging from $\text{Ca}_{0.48}\text{Mn}_{4.56}(\text{Si}_5\text{O}_{15})$ to $\text{Ca}_{1.58}\text{Mn}_{3.41}(\text{Si}_5\text{O}_{15})$ as well as minor amounts of Fe (up to 0.32 *apfu*), Mg (up to 0.14 *apfu*) and Al (0.06 *apfu*). Microthermometry of fluid inclusions hosted by johannsenite, rhodonite, sphalerite, calcite and Mn-calcite determined that the mineralization precipitated from fluids of low salinity (1.4 to 5.3 wt. % NaCl eq.) and moderate homogenization temperatures (187–318 °C), with a trend of simultaneous decrease in salinity and temperature, interpreted as mixing of fluids. Boiling of fluids was recorded in early calcite at temperatures from 275 to 279 °C, corresponding to pressure from 58 to 62 bars and paleodepth from 704 to 752 m. These values are similar to data from other post-caldera veins in the vicinity of the mine, as well as from other johannsenite-bearing epithermal deposits in the world.

Keywords: johannsenite, rhodonite, manganese, fluid inclusions, epithermal, gold, Rozália mine, Slovakia

Received: 4 May 2022; **accepted:** 12 May 2023; **handling editor:** J. Zachariáš

1. Introduction

Epithermal deposits of intermediate-sulfidation type are important sources of precious and base metals in the world. They are usually relatively young (Cenozoic, mainly Miocene) and related to the calc-alkaline magmatism developed in compressional, neutral, or extensional stress settings (Wang et al. 2019). Such deposits have variable content of base and precious metals (Ag–Pb–Zn–Cu, Au–Ag, Ag–Au), typically represented by minerals like pyrite, sphalerite, galena, chalcopyrite, tetrahedrite/tennantite, electrum, gold, acanthite, Au–Ag tellurides, and Ag-sulfosalts. Gangue minerals include quartz, carbonates, and adularia. A characteristic feature is also the increased manganese content, typically manifested by rhodonite, rhodochrosite, and Mn-calcite (Sillitoe and Hedenquist 2003; Simmons et al. 2005; Camprubí and Albinson 2007). Rarely, the Mn-rich py-

roxene johannsenite is also present as a gangue mineral (e.g., Smith et al. 1982; Sugaki et al. 1985; Shimizu et al. 1998; Echavarría et al. 2006; Subandrio and Basuki 2010; Reyes et al. 2016).

The area of the Middle Miocene Štiavnica stratovolcano hosts one of the world-famous examples of intermediate-sulfidation style of epithermal deposits and this ore field belongs to the largest ore districts in the Carpathian arc. Several of these deposits also contain manganese mineralization, typically represented by Mn-carbonates and rhodonite (e.g., Koděra 1955; Kovalenker et al. 1991; Kubač et al. 2018). Recently, a new, unusual type of epithermal manganese mineralization with abundant johannsenite was discovered during the exploration activities at the Rozália mine, which hosts several types of epithermal mineralization, including the Au–Ag–Pb–Zn–Cu epithermal deposit (called Banská Hodruša). This paper is focused on the detailed mineralogical and

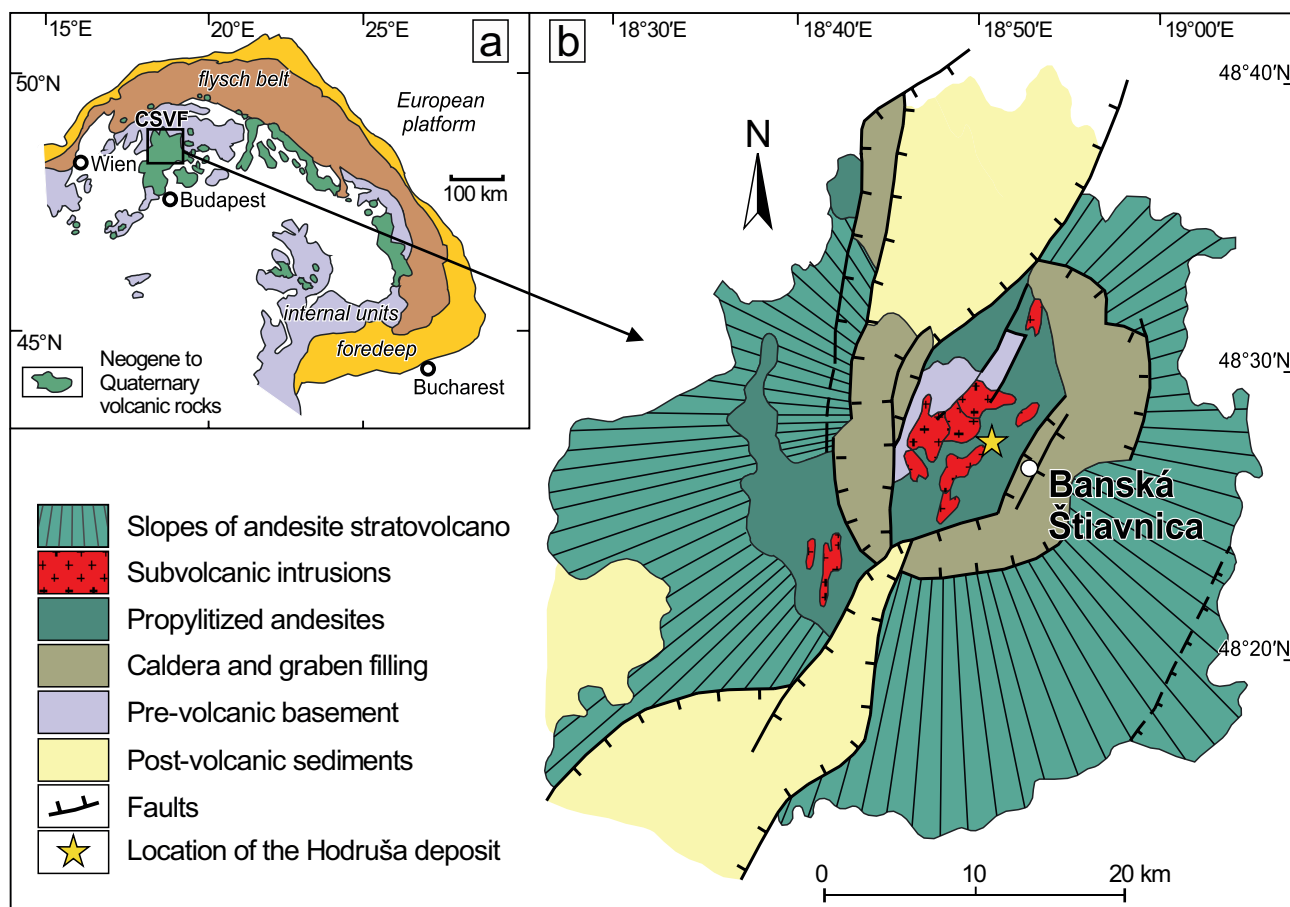


Fig. 1 Regional geological setting of the Rozália mine (after Lexa et al. 1999): **a** – Position of the Central Slovakia Volcanic Field (CSVF) within the Neogene to Quaternary volcanics of the Carpathian arc and Pannonian basin. **b** – Simplified structural scheme of the Štiavnica stratovolcano with location of the studied mine.

genetic characterization of the johannsenite-bearing mineralization. Comparison to other types of epithermal manganese mineralization in the Štiavnica stratovolcano is also provided.

2. Geological setting

The Rozália mine in the Hodruša-Hámre village is hosted by the central zone of the Štiavnica andesitic stratovolcano, which is a part of the Central Slovakia Volcanic Field, located on the inner side of the Carpathian arc (Fig. 1). An extensive caldera of 20 km in diameter, a voluminous subvolcanic intrusive complex, and a late-stage resurgent horst in the caldera centre accompanied by rhyolite volcanism are the most characteristic features of this volcano (Konečný et al. 1995). This volcano hosts the Banská Štiavnica–Hodruša precious and base metals ore district, which is one of the largest in the Carpathian arc (Lexa et al. 1999). This district contains various types of hydrothermal ore mineralization, ranging from early intrusion-related, subvolcanic skarns, base metal

stockwork, and porphyry Cu-Au systems to late, high-level, base- and precious-metal epithermal veins (Lexa et al. 1999).

The epithermal veins were formed during two major stages of the stratovolcano evolution. The early subhorizontal system of intermediate-sulfidation veins developed during the pre-caldera stage of the volcano and is known at the moment only from the Rozália mine. This vein system is hosted by a low angle shear zone, related to a quick exhumation of the subvolcanic granodiorite pluton, probably accompanied by a sector collapse of the hosting stratovolcano (Kubač et al. 2018). The later post-caldera stage veins of intermediate- to low-sulfidation type are associated with the long-lasting uplift of the resurgent horst in the centre of the caldera. This extensive epithermal system includes ~120 veins, covering almost 100 km² (Lexa et al. 1999), including the Rozália mine. In the stratovolcano, both systems locally contain some form of manganese mineralization, however, at the Rozália mine it was known yet just from pre-caldera veins.

The Rozália mine was used to exploit three different types of ores, subsequently mined during the history of

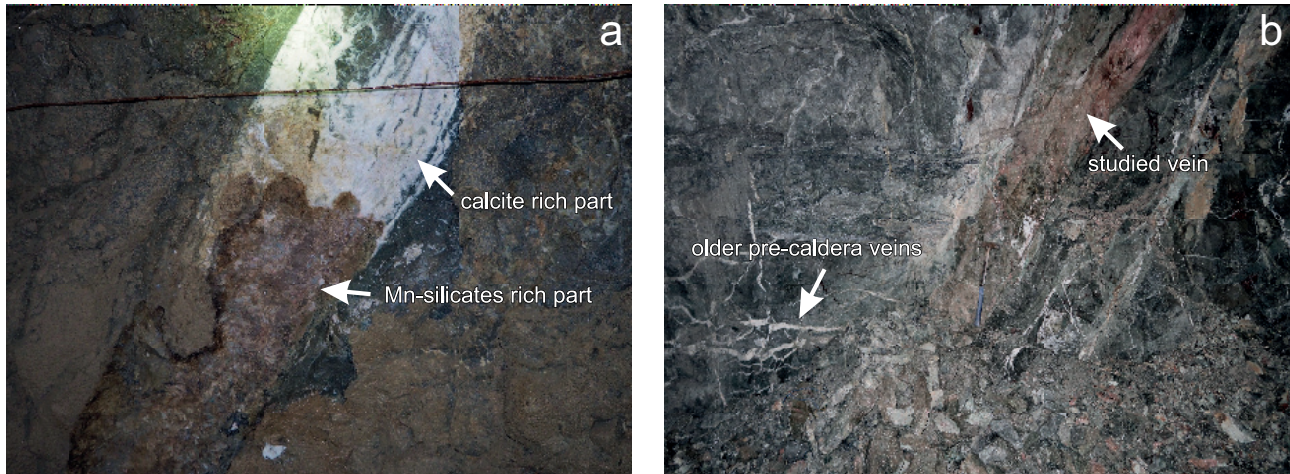


Fig. 2 Photographs of the studied Mn-rich vein, hosted by andesite: **a** – Sampled vein that consists of two contrasting parts, represented by brown Mn-rich mineralization and by white calcite mass in the upper part of the image. Calcite hosts sporadic black veinlets and green spots of altered host rocks fragments. The field of view is approximately 1 m. **b** – Crosscut relationship of the brown, steep Mn-rich vein with older shallow-dipping pre-caldera veins. The field of view is approximately 3 m.

the mine: from 1951 to 1991 the late post-caldera Cu–Pb–Zn veins, from 1991 to 1992 the base metal stockwork ores and from 1992 until today the pre-caldera Au–Ag–Pb–Zn–Cu veins (Koděra et al. 2005; Kubač et al. 2018). At this mine, the post-caldera veins have an average dip of 50–70° to SE and belong to the system of NE–SW oriented veins related to the resurgent horst uplift. In the entire district, Koděra (1963) and Kovalenker et al. (1991) have distinguished 5 mineralization stages and four vertical zones in the post-caldera veins. The Mn-mineralization in these veins occurs mainly in the upper Pb–Zn zone in the 3rd rhodonite–carbonate–quartz stage, represented by rhodonite, rhodochrosite, Mn-calcite, and kutnohorite. However, in the Rozália mine, this type of veins hosts predominantly the 4th galena–chalcopryrite and the 5th sulfosalt–baryte stages in the lowest lower Pb–Zn and Cu zones and contains no Mn-bearing minerals. The major veins (Rozália, Bakali, Amália, Martin and Ochsenkopf) typically consist of coarse-grained base-metal sulfides, various Cu–Pb–Bi–Ag sulfosalts, and acanthite (Jeleň et al. 2012; Sejkora et al. 2015; Chovan et al. 2019).

The pre-caldera vein system occurs between the 10th and 19th horizons of the Rozália mine and it is segmented by the steeply-dipping post-caldera veins and faults of the resurgent horst (Koděra et al. 2005; Kubač et al. 2018). The Mn-mineralization occurs in the early paragenetic stage, related to the early development of the shear zone (Karolína vein system), and hosted by E–W and ESE–WNW fractures, dipping 40–60° to the south. The Mn-rich mineral assemblage typically forms brecciated texture (rarely banded texture), where andesite fragments are cemented by pinkish Mn minerals (rhodonite, rhodochrosite, Mn-calcite), accompanied by chlorite and grey quartz. Minor dolomite and siderite

are also present. Minerals of Mn precipitated prior to the main sulfide and gold accumulation, represented by sphalerite, galenite, chalcopryrite, pyrite, electrum, and Au–Ag tellurides (hessite and petzite; Kubač et al. 2018). In later paragenetic stages, corresponding to the late development of the shear zone, Mn-bearing minerals are nearly absent. These later stages include thin NNE–SSW oriented quartz–gold veins with medium dip (~45° to SE) in tension cracks inside the shear zone (Křištof vein system) and complementary detachment-hosted, shallow-dipping (~30° to ESE), quartz–base metals–gold veins of NNE–SSW orientation in the roof of shear zone (Agnesa vein system; Kubač et al. 2018).

The base-metal stockwork mineralization is the oldest type of ore mineralization in the mine, developed in the roof of altered porphyritic granodiorite intrusion between the Rozália and Bakali post-caldera veins on the 8th horizon of the mine (Štohl et al. 1994; Koděra et al. 2004). Accompanying hydrothermal alteration has increased Mn concentration, mainly present in chlorite (up to 1.7 wt. % MnO) and epidote (up to 0.9 wt. % MnO) (Koděra et al. 2004).

The new type of manganese vein mineralization with abundant johannsenite was discovered at the 18th horizon of the Rozália mine (176 m a.s.l.) hosted by andesite (Fig. 2). Vein filling consists of two contrasting parts, represented by brown manganese mineralization and by white calcite mineralization hosting sporadic black veinlets (Fig. 3b), with a sharp contact between both parts (Fig. 2a). According to the crosscutting relationship with a shallow-dipping pre-caldera vein (Agnesa-type vein) it belongs to the post-caldera vein system (Fig. 2b). Furthermore, the studied vein occurs on a NE–SW oriented fracture dipping 55° to the southeast, which is characteristic for most post-caldera veins. However, mineral-

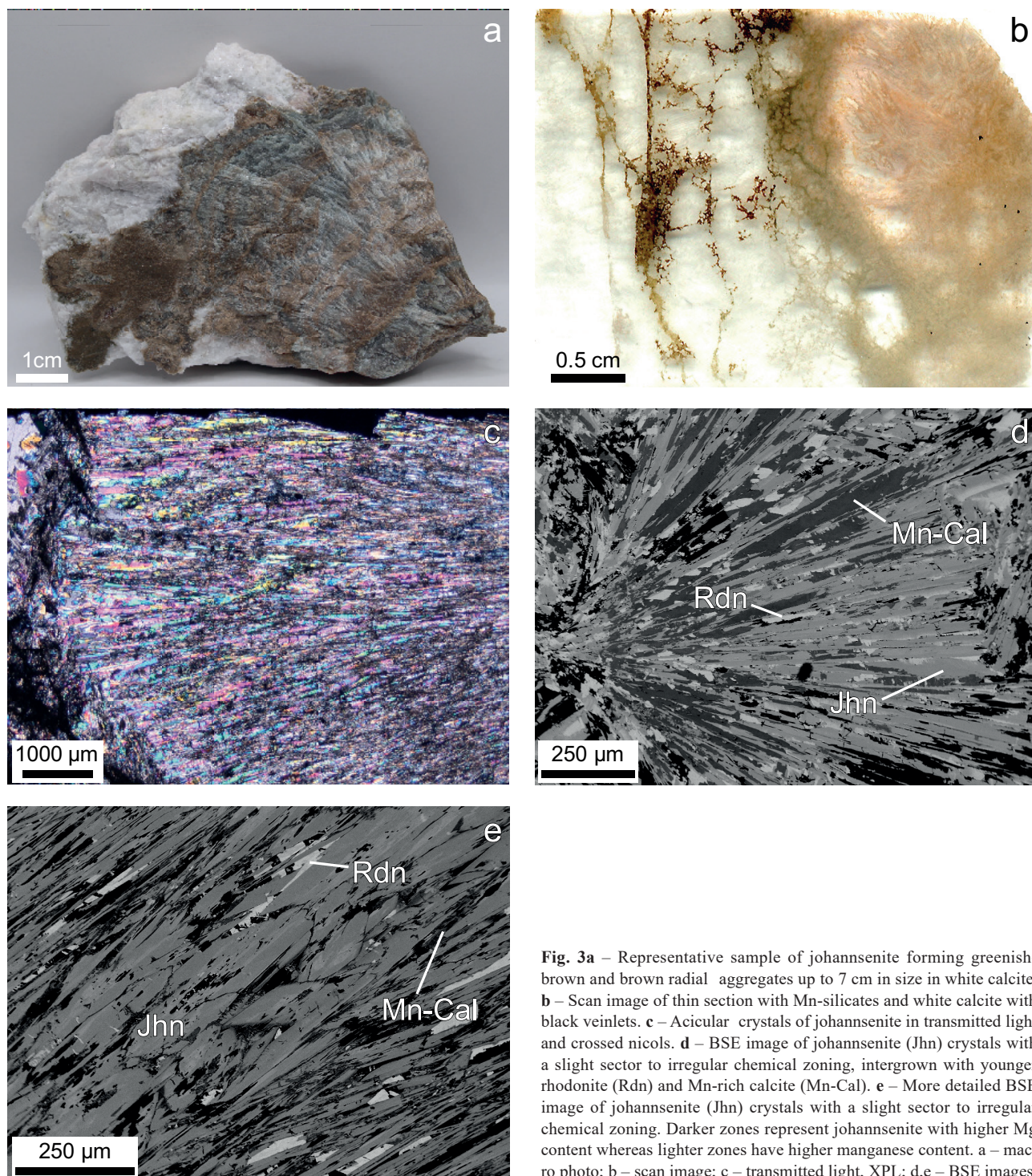


Fig. 3a – Representative sample of johannsenite forming greenish-brown and brown radial aggregates up to 7 cm in size in white calcite. **b** – Scan image of thin section with Mn-silicates and white calcite with black veinlets. **c** – Acicular crystals of johannsenite in transmitted light and crossed nicols. **d** – BSE image of johannsenite (Jhn) crystals with a slight sector to irregular chemical zoning, intergrown with younger rhodonite (Rdn) and Mn-rich calcite (Mn-Cal). **e** – More detailed BSE image of johannsenite (Jhn) crystals with a slight sector to irregular chemical zoning. Darker zones represent johannsenite with higher Mg content whereas lighter zones have higher manganese content. **a** – macro photo; **b** – scan image; **c** – transmitted light, XPL; **d,e** – BSE images.

ogically the vein is quite unique and its mineralogical properties and genesis are discussed further in text.

3. Analytical methods

Quantitative chemical analyses of minerals were performed using a Cameca SX100 and JEOL JXA-8530F

electron probe micro-analyser (EPMA). Operating conditions for Cameca SX100 (State Geological Institute of Dionýz Štúr, Bratislava, Slovakia) in WDS mode for sulfides were 25 kV, 10 nA and 1–9 µm beam diameter. The following standards and X-ray lines were used: Ag (AgL_α), Bi (BiL_α), Bi_2Se_3 (SeL_β), $CuFeS_2$ (CuK_α , FeK_α , SK_α), Co (CoK_α), GaAs (AsL_α), Ni (NiK_α), PbS (PbM_α), Sn (SnL_β), ZnS (ZnK_α). For silicates and carbonates,

the following conditions were used: 15 kV, 20 nA and 1–9 μm wide beam and standards and X-ray lines were as follows: Al_2O_3 (AlK_α), albite (NaK_α), barite (SK_α), CaF_2 (FK_α), Cr (CrK_α), fayalite (FeK_α), forsterite or MgO (MgK_α), forsterite, SiO_2 or orthoclase (SiK_α), NaCl (ClK_α), Ni (NiK_α), orthoclase (KK_α), rhodonite (MnK_α), TiO_2 (TiK_α) and wollastonite (CaK_α).

Operating conditions for JEOL JXA-8530FE (Earth Science Institute, Slovak Academy of Sciences, Banská Bystrica, Slovakia) for sulfides were 20 kV, 16 nA and 5–10 μm beam diameter. The following standards and X-ray lines were used: Ag (AgL_α), arsenopyrite (AsL_β), Au (AuM_α), bismuth (BiL_α), bismuthinite (BiM_β), Bi_2Se_3 (SeL_α or SeL_β), CdS (CdL_α), CdTe (TeL_α), chalcopyrite (CuK_α), cinnabar (HgM_α), cobaltite (CoK_α), GaAs (AsL_β), galena (PbM_α), gersdorffite (NiK_α), pyrite (FeK_α , SK_α), rhodonite (MnK_α), sphalerite (ZnK_α), stibnite (SbL_α). Operating wave-dispersive (WDS) mode for silicates was 15 kV, 20 nA and 5–10 μm wide beam and standards and X-ray lines were as follows: albite (NaK_α), apatite (PK_α), Cr_2O_3 (CrK_α), diopside (CaL_α , MgK_α , SiK_α), hematite (FeK_α), Ni_2Si (NiK_α), orthoclase (AlK_α , KK_α), rhodonite (MnK_α), rutile (TiK_α), ScVO_4 (ScK_α , VK_α). Operating wave-dispersive (WDS) mode for carbonates was 15 kV, 16 nA, 10 μm wide beam and the following standards and X-ray lines were used: albite (AlK_α , NaK_α), baryte (BaL_α), celestite (SrL_α), diopside (CaK_α , MgK_α , SiK_α), hematite (FeK_α), rhodonite (MnK_α).

Microthermometric study of fluid inclusions was performed on representative samples of vein filling, and it was preceded by a petrographic study of fluid inclusions. The measurements were conducted using a Linkam THMSG-600 stage mounted on an Olympus BX-53 microscope (Department of Mineralogy, Petrology and Economic Geology, Faculty of Natural Sciences Comenius University in Bratislava). Calibration of the instrument was performed with natural inclusions (CO_2 , H_2O) and synthetic $\text{K}_2\text{Cr}_2\text{O}_7$. The measurement error at subambient temperatures (–100 to 25 °C) is estimated to be ± 0.2 °C, at higher temperature (up to 300 °C) to ± 1.0 °C. Salinity was calculated from ice melting temperatures according to Bodnar (1993).

As the optical properties of minerals in thick wafers used for the microthermometry of fluid inclusion often did not allow to reliably identify their host mineral, Raman spectroscopy was applied. The study was performed on a DXR Raman microscope with OMNIC spectroscopic software (University Science Park, Comenius University in Bratislava, Slovakia). The bands from a polystyrene standard were used to calibrate the spectrometer. Silicates were measured with a 532 nm laser at 7 kW and an aperture of 50 μm pinhole. Carbonates and sphalerite were measured with a 633 nm laser, 8 kW power and a 50 nm pinhole aperture. A magnification of 100 \times and an exposure time of 2 min were used for all measurements. The measurements had a spectral range of 1800–50 cm^{-1} , the resolution was 1 cm^{-1} .

A representative sample of the manganese-rich and sulfide free part of the vein was analysed by one whole rock analysis. Gold was analysed using fire assay method with gravimetric finish in the laboratories of ALS CHE-MEX Rosia Montana in Romania (methodology code Au-GRA21). Other 48 elements were analysed by aqua regia digestion with ICP-MS finish (analytical code ME-MS61). Details of the methods, including detection limits, are available at <https://www.alsglobal.com>.

4. Results

4.1. Mineralogical characteristics

The studied vein with manganese mineralization has the thickness up to 30 cm. It has massive texture, hosting greenish, pink and brown manganese silicates, which locally transforms to a typical radial texture. Manganese mineralization is represented by abundant johannsenite in association with younger rhodonite, and minor Mn-rich calcite. Locally can be found coarse-grained white calcite, which can contain very thin macroscopically black veinlets. These veinlets typically consist of microcrystalline clinozoisite associated with subordinate amounts of rhodochrosite in intergranular positions. Other gangue minerals are quartz, chlorite, adularia, and fluorapatite. An assemblage of ore minerals represented by sphalerite, galena, pyrite, chalcopyrite, and acanthite was found exclusively in the Mn-rich part of the vein, forming irregularly interspersed grains in cavities of johannsenite, later filled by Mn-rich calcite. Whole rock analyses of the Mn-rich part of the studied vein provided following concentrations of selected elements: Au 0.05 ppm, Ag 3.4 ppm, Al 2.7 %, Ca 9.7 %, Cd 45.2 ppm, Cu 42.4 ppm, Fe 2.3 %, K 2.7 %, Mg 0.81 %, Mn >10 %, Na 0.06 %, Pb 4670 ppm, S 1.17 %, Te 0.82 ppm and Zn 7900 ppm.

4.2. Silicates

4.2.1. Johannsenite

Johannsenite is the most abundant and paragenetically the oldest mineral in the Mn-rich part of the vein. It forms greenish-blue, greenish-brown or brown (caused by oxidation of Mn) radial aggregates reaching up to 7 cm in size (Figs 3a,c), which consist of individual acicular crystals. Aggregates and crystals of johannsenite are often intimately intergrown with younger rhodonite and Mn-rich calcite (Figs 3d,e). Only very slight sector to irregular chemical zoning was observed in johannsenite using BSE mode (Fig. 3e). Very fine-grained aggregates and intergrowths of johannsenite and rhodonite have also been observed.

Tab. 1 Representative chemical analyses of johannsenite (in wt. %).

| | 1 | 2 | 3 | 4 | 5 | 6 | 7 | 8 | 9 | 10 | 11 | 12 | 13 | 14 | 15 |
|--------------------------------|-------|-------|-------|--------|-------|--------|-------|-------|-------|-------|--------|-------|--------|--------|--------|
| Na ₂ O | 0.09 | 0.07 | 0.16 | 0.00 | 0.19 | 0.08 | 0.07 | 0.00 | 0.15 | 0.00 | 0.00 | 0.00 | 0.00 | 0.00 | 0.00 |
| CaO | 21.51 | 21.63 | 21.79 | 22.15 | 21.66 | 22.22 | 22.81 | 20.07 | 20.36 | 20.41 | 21.99 | 20.89 | 22.20 | 22.16 | 22.49 |
| MgO | 1.46 | 1.17 | 0.99 | 0.80 | 1.11 | 1.54 | 1.91 | 2.16 | 2.87 | 0.70 | 0.56 | 0.17 | 0.26 | 1.56 | 1.61 |
| MnO | 26.80 | 27.82 | 27.08 | 28.34 | 26.88 | 26.56 | 23.38 | 25.05 | 24.70 | 30.66 | 28.91 | 31.03 | 29.65 | 26.94 | 26.85 |
| FeO | 1.03 | 0.80 | 0.88 | 0.82 | 0.89 | 0.61 | 1.73 | 1.94 | 2.09 | 0.38 | 0.47 | 0.35 | 0.61 | 0.78 | 0.75 |
| Al ₂ O ₃ | 0.66 | 0.51 | 0.48 | 0.08 | 0.66 | 0.78 | 0.75 | 0.93 | 1.10 | 0.06 | 0.07 | 0.00 | 0.07 | 0.21 | 0.25 |
| SiO ₂ | 47.64 | 47.91 | 48.00 | 48.15 | 47.61 | 48.82 | 49.00 | 48.40 | 48.03 | 47.49 | 48.12 | 47.54 | 47.34 | 48.39 | 48.18 |
| total | 99.18 | 99.91 | 99.38 | 100.33 | 99.01 | 100.60 | 99.65 | 98.56 | 99.29 | 99.71 | 100.12 | 99.99 | 100.13 | 100.05 | 100.13 |
| Na ⁺ | 0.007 | 0.006 | 0.013 | 0.000 | 0.015 | 0.006 | 0.006 | 0.000 | 0.012 | 0.000 | 0.000 | 0.000 | 0.000 | 0.000 | 0.000 |
| Ca ²⁺ | 0.952 | 0.953 | 0.963 | 0.975 | 0.961 | 0.964 | 0.991 | 0.884 | 0.891 | 0.909 | 0.971 | 0.931 | 0.986 | 0.971 | 0.986 |
| Σ | 0.958 | 0.959 | 0.976 | 0.975 | 0.976 | 0.970 | 0.997 | 0.884 | 0.902 | 0.909 | 0.971 | 0.931 | 0.986 | 0.971 | 0.986 |
| Mg ²⁺ | 0.090 | 0.072 | 0.061 | 0.049 | 0.068 | 0.093 | 0.116 | 0.132 | 0.175 | 0.044 | 0.034 | 0.010 | 0.016 | 0.095 | 0.098 |
| Mn ²⁺ | 0.937 | 0.969 | 0.946 | 0.986 | 0.942 | 0.911 | 0.803 | 0.872 | 0.854 | 1.079 | 1.009 | 1.093 | 1.041 | 0.933 | 0.930 |
| Fe ²⁺ | 0.035 | 0.028 | 0.030 | 0.028 | 0.031 | 0.021 | 0.059 | 0.067 | 0.071 | 0.013 | 0.016 | 0.012 | 0.021 | 0.027 | 0.026 |
| Σ | 1.063 | 1.068 | 1.037 | 1.063 | 1.042 | 1.024 | 1.078 | 1.071 | 1.101 | 1.136 | 1.059 | 1.115 | 1.079 | 1.055 | 1.054 |
| Al ³⁺ | 0.032 | 0.025 | 0.023 | 0.004 | 0.032 | 0.037 | 0.036 | 0.045 | 0.053 | 0.003 | 0.003 | 0.000 | 0.003 | 0.010 | 0.012 |
| Si ⁴⁺ | 1.967 | 1.970 | 1.979 | 1.978 | 1.971 | 1.976 | 1.987 | 1.989 | 1.962 | 1.974 | 1.982 | 1.977 | 1.963 | 1.978 | 1.971 |
| Σ | 1.999 | 1.994 | 2.003 | 1.982 | 2.003 | 2.014 | 2.023 | 2.034 | 2.015 | 1.977 | 1.986 | 1.977 | 1.966 | 1.988 | 1.983 |

calculated empirical formulae are based on sum of O atoms = 6 *apfu*

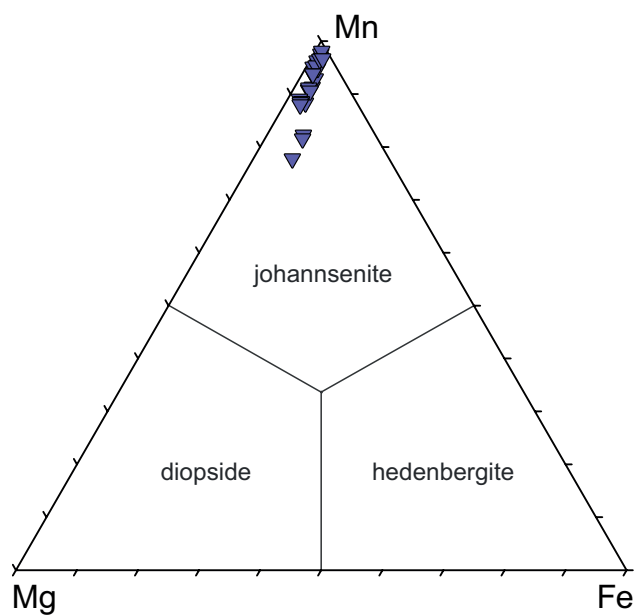


Fig. 4 The chemical composition of johannsenite from the Rozália mine in the ternary plot Mn-Mg-Fe (in *apfu*).

Representative spot chemical analyses of johannsenite and the corresponding calculated empirical formulae are shown in Tab. 1. Chemical composition of johannsenite from the Rozália mine is distinguished with slightly elevated contents of Mg (reaching up to 0.17 *apfu*) substituting for Mn (Fig. 4). Minor amounts of Fe (up to 0.07 *apfu*), Al (up to 0.04 *apfu*) and Na (up to 0.01 *apfu*) were also detected in studied samples. The average ($n=23$) empirical formula of johannsenite from the Rozália mine based on $O=6$ is $\text{Ca}_{0.96}(\text{Mn}_{0.97}\text{Mg}_{0.07}\text{Fe}_{0.03})_{1.07}(\text{Si}_{1.98}\text{Al}_{0.02})_{2.00}\text{O}_6$.

Representative Raman spectra of johannsenite from the Rozália mine (Fig. 5) are distinguished by one intense band at 1011 cm^{-1} related to antisymmetric Si–O–Si vibration. Less intense bands at 904 cm^{-1} and $843\text{--}844\text{ cm}^{-1}$ are probably related to antisymmetric Si–O–Si vibrations. Similar bands are also described by Makreski et al. (2005) and Huang et al. (2000) for other clinopyroxenes. Another band is at $651\text{--}652\text{ cm}^{-1}$ is related to the Si–O–Si bending. Less intense bands were observed at 1030 cm^{-1} , 549 cm^{-1} , $372\text{--}373\text{ cm}^{-1}$, $334\text{--}335\text{ cm}^{-1}$ and in the $301\text{--}120\text{ cm}^{-1}$ region and are related to the Mn–O and Ca–O stretching or displacement. The effect of the crystal orientation on the spectra was manifested mainly by different vibrational intensities of peaks in the $300\text{--}400\text{ cm}^{-1}$ region (Mernagh and Hoatson 1997). The obtained Raman spectra of johannsenite from the Rozália mine correspond to the typical johannsenite spectra published by Makreski et al. (2005).

4.2.2. Rhodonite, vittinkiite

Rhodonite is the second most common mineral in the studied part of the vein. It predominantly occurs as sub-

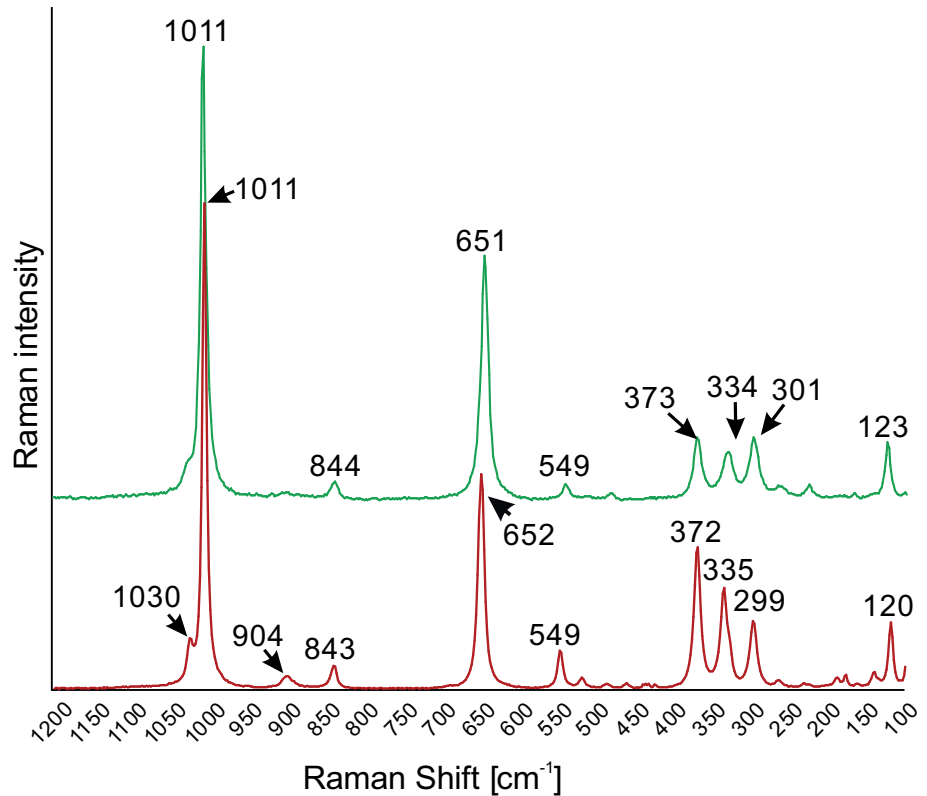


Fig. 5 – Typical Raman spectra of johannsenite from the Rozália mine, presented as a compilation of two spectra. The lower was recorded after 90° turn to evaluate the effect of crystallographic orientation. Numbers mark the position of main bands.

hedral to euhedral crystals and aggregates intimately intergrown with johannsenite and Mn-rich calcite (Fig. 6a). Rhodonite forms euhedral crystals up to 1 mm in size (Fig. 6b), growing in empty cavities, which were later filled with sulfides and Mn-rich calcite. It is younger than johannsenite and it often shows relatively strong, sector to oscillatory chemical zoning caused by the variation of Ca and Mn contents.

Representative quantitative chemical analyses of rhodonite are shown in Tab. 2. There is a strong com-

positional variation of Ca versus Mn contents (Fig. 7), ranging from $\text{Ca}_{0.48}\text{Mn}_{4.56}(\text{Si}_5\text{O}_{15})$ to $\text{Ca}_{1.58}\text{Mn}_{3.41}(\text{Si}_5\text{O}_{15})$, which covers practically the entire field of rhodonite as defined in the mineral classification of the rhodonite group (Shchipalkina et al. 2019, 2020). One Ca-poor spot corresponds to recently defined member of the rhodonite group, vittinkiite, $\text{MnMn}_4(\text{Si}_5\text{O}_{15})$. Other, minor elements detected in rhodonite are Fe (up to 0.32 *apfu*), Mg (up to 0.14 *apfu*) and Al (up to 0.06 *apfu*).

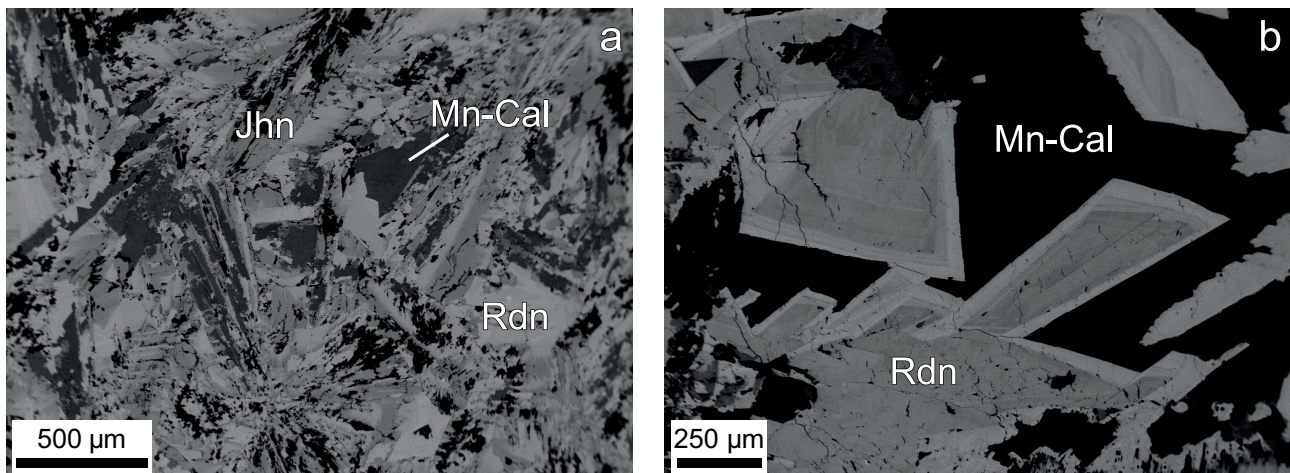


Fig. 6a – Aggregates of rhodonite (Rdn) intimately intergrown with darker johannsenite (Jhn) and Mn-rich calcite (Mn-Cal). **b** – Rhodonite (Rdn) euhedral crystals with oscillatory chemical zoning, crystallized in a cavity filled by Mn-rich calcite (Mn-Cal). Darker zones represent rhodonite with higher Ca content whereas lighter zones have higher manganese content. BSE images.

Tab. 2 Representative chemical analyses of rhodonite (in wt. %).

| | 1 | 2 | 3 | 4 | 5 | 6 | 7 | 8 | 9 | 10 | 11 | 12 | 13 | 14 | 15 |
|--------------------------------|-------|--------|-------|-------|-------|-------|--------|--------|-------|--------|-------|-------|-------|--------|-------|
| Na ₂ O | 0.00 | 0.00 | 0.00 | 0.00 | 0.10 | 0.09 | 0.00 | 0.00 | 0.00 | 0.00 | 0.00 | 0.00 | 0.00 | 0.00 | 0.00 |
| CaO | 5.93 | 11.82 | 4.81 | 7.36 | 13.94 | 18.38 | 5.04 | 5.72 | 12.23 | 6.91 | 4.74 | 6.89 | 8.42 | 6.89 | 4.09 |
| MgO | 0.29 | 0.24 | 0.36 | 0.68 | 0.21 | 0.93 | 0.34 | 0.55 | 0.23 | 0.23 | 0.12 | 0.17 | 0.30 | 0.62 | 0.32 |
| MnO | 46.76 | 40.98 | 47.21 | 44.55 | 38.16 | 31.69 | 47.58 | 47.06 | 40.48 | 46.67 | 47.08 | 43.80 | 40.84 | 44.39 | 49.21 |
| FeO | 1.25 | 0.44 | 1.71 | 1.32 | 0.43 | 0.76 | 1.36 | 1.20 | 0.29 | 0.74 | 1.33 | 1.90 | 3.54 | 2.55 | 1.87 |
| Al ₂ O ₃ | 0.18 | 0.44 | 0.05 | 0.05 | 0.20 | 0.44 | 0.14 | 0.08 | 0.21 | 0.12 | 0.19 | 0.08 | 0.00 | 0.04 | 0.06 |
| SiO ₂ | 45.29 | 46.37 | 45.32 | 45.99 | 46.85 | 47.56 | 46.31 | 45.82 | 45.94 | 46.27 | 46.28 | 45.63 | 46.57 | 45.65 | 44.44 |
| total | 99.68 | 100.29 | 99.46 | 99.96 | 99.89 | 99.85 | 100.78 | 100.42 | 99.39 | 100.95 | 99.74 | 98.47 | 99.67 | 100.15 | 99.99 |
| Na ⁺ | 0.000 | 0.000 | 0.000 | 0.000 | 0.021 | 0.017 | 0.000 | 0.000 | 0.000 | 0.000 | 0.000 | 0.000 | 0.000 | 0.000 | 0.000 |
| Ca ²⁺ | 0.688 | 1.341 | 0.561 | 0.847 | 1.576 | 2.043 | 0.578 | 0.658 | 1.402 | 0.790 | 0.547 | 0.804 | 0.966 | 0.795 | 0.479 |
| Mg ²⁺ | 0.046 | 0.038 | 0.058 | 0.109 | 0.034 | 0.145 | 0.055 | 0.089 | 0.037 | 0.037 | 0.019 | 0.028 | 0.048 | 0.100 | 0.052 |
| Mn ²⁺ | 4.295 | 3.676 | 4.351 | 4.048 | 3.412 | 2.786 | 4.311 | 4.283 | 3.668 | 4.216 | 4.299 | 4.041 | 3.702 | 4.045 | 4.561 |
| Fe ²⁺ | 0.113 | 0.039 | 0.156 | 0.119 | 0.038 | 0.066 | 0.122 | 0.108 | 0.026 | 0.066 | 0.120 | 0.173 | 0.317 | 0.229 | 0.171 |
| Σ | 5.143 | 5.094 | 5.126 | 5.123 | 5.081 | 5.057 | 5.065 | 5.138 | 5.133 | 5.109 | 4.986 | 5.046 | 5.032 | 5.169 | 5.263 |
| Al ³⁺ | 0.023 | 0.055 | 0.007 | 0.007 | 0.025 | 0.053 | 0.018 | 0.010 | 0.026 | 0.015 | 0.024 | 0.010 | 0.000 | 0.006 | 0.008 |
| Si ⁴⁺ | 4.911 | 4.911 | 4.932 | 4.934 | 4.946 | 4.936 | 4.954 | 4.923 | 4.914 | 4.934 | 4.989 | 4.970 | 4.984 | 4.911 | 4.862 |
| Σ | 4.934 | 4.967 | 4.939 | 4.940 | 4.971 | 4.989 | 4.972 | 4.933 | 4.940 | 4.949 | 5.013 | 4.980 | 4.984 | 4.917 | 4.870 |

calculated empirical formulae are based on sum of O atoms = 15 apfu

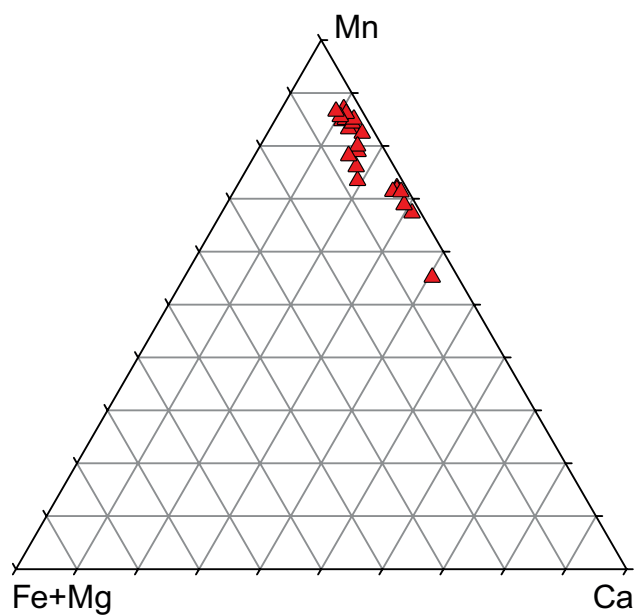


Fig. 7 The chemical composition of rhodonites in a ternary plot, showing strong compositional variation of Ca versus Mn content.

4.3. Carbonates

4.3.1. Calcite

Two types of calcite were distinguished. The first type forms the main mass of the white part of the vein (Fig. 3a). It is mostly coarse-grained and contains only a minor amount of Mn, up to 0.02 apfu. Locally, especially where black clinozoisite-rhodochrosite veinlets are present, rare outer Mn-rich zones are overgrown on calcite grains with Mn content up to 0.14 apfu (Fig. 8a).

The second, probably younger type of calcite is represented by white to light pink Mn-rich calcite which mostly forms fine-grained, but occasionally also coarse-grained aggregates, filling interstitial spaces or cavities in johannsenite–rhodonite aggregates (Fig. 6b). They are probably coeval with Mn-rich zones in the main calcite mass of the vein. In the cavities of Mn-silicate aggregates, Mn-calcite is locally associated with sphalerite, galena, and pyrite as well as with minor amounts of quartz. The Mn content in this type of calcite is ranging from 0.08 to 0.29 apfu. Representative chemical analyses of calcites are shown in Tab. 3.

4.3.2. Rhodochrosite

Rhodochrosite only occurs in black veinlets developed in the main mass of white of calcite. Aggregates of rhodochrosite fill intergranular spaces between subhedral grains and crystals of clinozoisite (Fig. 8b). Quantitative chemical analyses of rhodochrosite are shown in Tab. 3. Along with the dominant content of Mn, Ca content (ranging

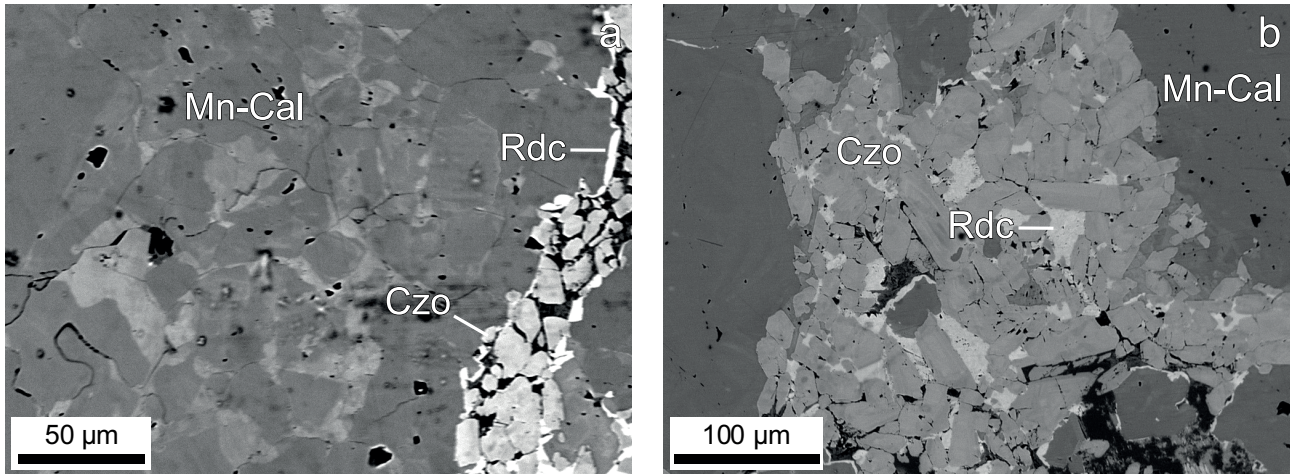


Fig. 8a – Younger black veinlets hosted by main mass of coarse-grained white calcite (Mn-Cal) with irregular chemical zoning. Darker zones represent calcite with higher Ca content whereas lighter zones have higher manganese content. **b** – More detailed BSE image of younger veinlets with clinozoisite (Czo) anhedral grains and rhodochrosite (Rdc) in intergranular positions. BSE images.

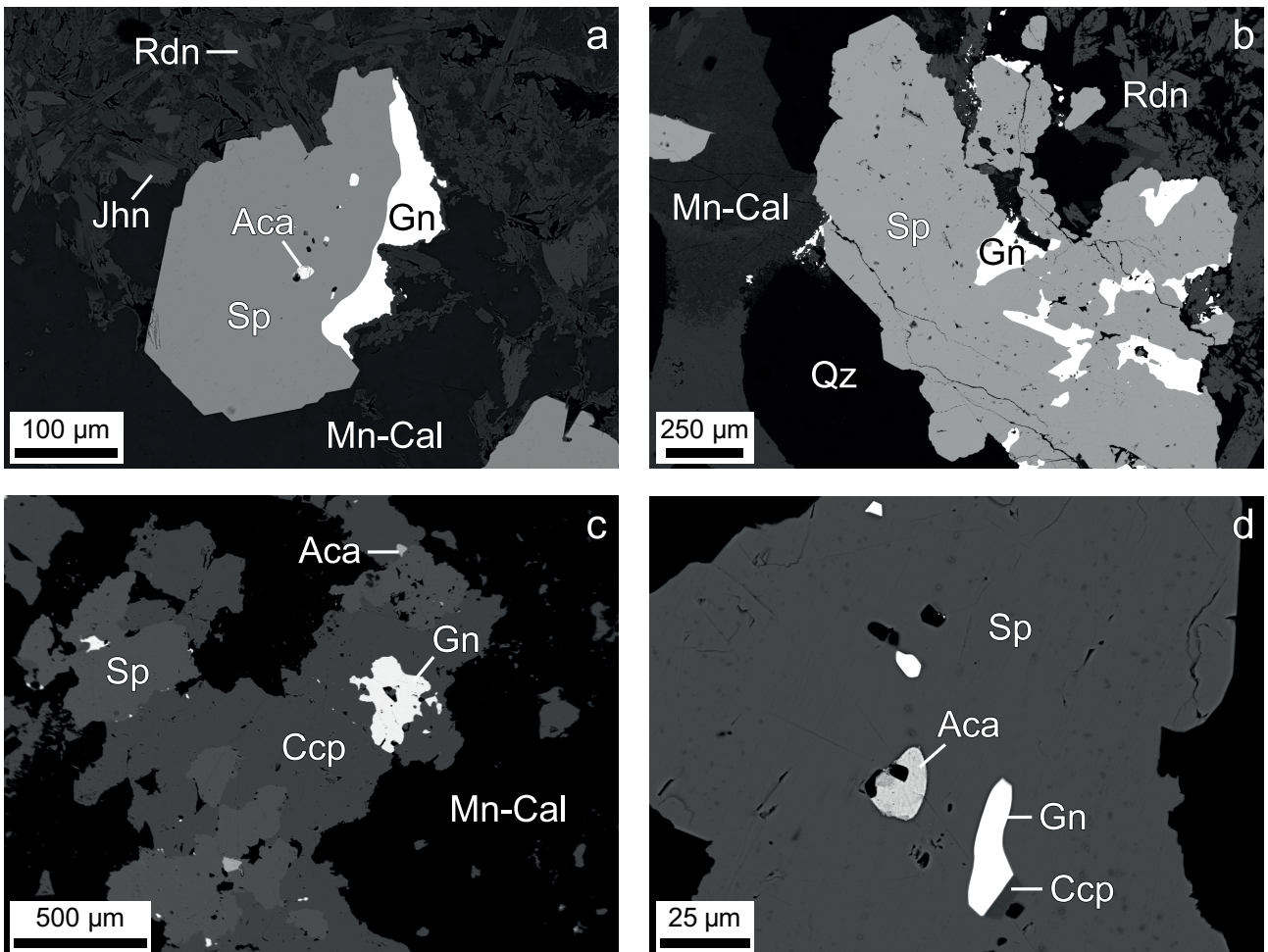


Fig. 9a – Subhedral grain of sphalerite (Sp) with acanthite inclusions (Aca) and galena (Gn), surrounded by johannsenite (Jhn), rhodonite (Rdn) and Mn-calcite (Mn-Cal). **b** – Anhedral grain of sphalerite (Sp) intergrown with galena (Gn), situated in rhodonite (Rdn) and quartz (Qz), which about a cavity filled with Mn-calcite (Mn-Cal). **c** – Anhedral inclusions of galena (Gn) and acanthite (Aca) situated in aggregates of sphalerite (Sp) and chalcopyrite (Ccp). **d** – More detailed BSE image of acanthite (Aca), galena (Gn) and chalcopyrite (Ccp) inclusions in a sphalerite (Sp) grain. BSE images.

Tab. 3 Representative chemical analyses of calcite and rhodochrosite (in wt. %). Analyses 1-5: calcite from Mn-rich part, 6-8: calcite from white part.

| | 1 | 2 | 3 | 4 | 5 | 6 | 7 | 8 | 9 | 10 | 11 | 12 | 13 | 14 | 15 |
|------------------|--------|-------|-------|-------|-------|--------|--------|--------|-------|-------|-------|-------|-------|-------|-------|
| | Cal | Cal | Cal | Cal | Cal | Cal | Cal | Cal | Rds |
| CaO | 51.20 | 48.13 | 55.45 | 41.75 | 36.91 | 62.20 | 60.87 | 50.56 | 7.42 | 8.41 | 6.29 | 10.55 | 16.99 | 12.61 | 19.37 |
| MnO | 5.36 | 7.83 | 0.28 | 13.05 | 19.49 | 0.29 | 3.69 | 10.84 | 45.29 | 44.54 | 49.21 | 48.06 | 40.65 | 47.05 | 38.31 |
| SrO | 0.03 | 0.08 | 0.03 | 0.01 | 0.01 | 0.14 | 0.04 | 0.05 | 0.03 | 0.00 | 0.02 | 0.00 | 0.02 | 0.00 | 0.00 |
| MgO | 0.06 | 0.04 | 0.02 | 0.32 | 0.08 | 0.24 | 0.02 | 0.07 | 2.99 | 3.03 | 1.74 | 0.23 | 0.29 | 0.25 | 0.24 |
| FeO | 0.02 | 0.05 | 0.02 | 0.69 | 0.13 | 0.10 | 0.00 | 0.04 | 1.77 | 1.86 | 1.48 | 0.37 | 0.32 | 0.31 | 0.22 |
| CO ₂ | 43.59 | 42.74 | 43.73 | 41.64 | 41.23 | 49.37 | 50.10 | 46.54 | 38.28 | 38.68 | 38.28 | 38.57 | 39.07 | 39.55 | 39.37 |
| total | 100.25 | 98.88 | 99.53 | 97.47 | 97.85 | 112.33 | 114.72 | 108.11 | 95.77 | 96.52 | 97.02 | 97.78 | 97.35 | 99.76 | 97.52 |
| Ca ²⁺ | 0.922 | 0.884 | 0.995 | 0.787 | 0.703 | 0.989 | 0.953 | 0.853 | 0.152 | 0.171 | 0.129 | 0.215 | 0.341 | 0.250 | 0.386 |
| Mn ²⁺ | 0.076 | 0.114 | 0.004 | 0.194 | 0.293 | 0.004 | 0.046 | 0.145 | 0.734 | 0.714 | 0.797 | 0.773 | 0.645 | 0.738 | 0.604 |
| Sr ²⁺ | 0.000 | 0.001 | 0.000 | 0.000 | 0.000 | 0.001 | 0.000 | 0.000 | 0.000 | 0.000 | 0.000 | 0.000 | 0.000 | 0.000 | 0.000 |
| Mg ²⁺ | 0.001 | 0.001 | 0.000 | 0.008 | 0.002 | 0.005 | 0.001 | 0.002 | 0.085 | 0.086 | 0.050 | 0.006 | 0.008 | 0.007 | 0.007 |
| Fe ²⁺ | 0.000 | 0.001 | 0.000 | 0.010 | 0.002 | 0.001 | 0.000 | 0.001 | 0.028 | 0.029 | 0.024 | 0.006 | 0.005 | 0.005 | 0.003 |
| Σ | 1.000 | 1.000 | 1.000 | 1.000 | 1.000 | 1.000 | 1.000 | 1.000 | 1.000 | 1.000 | 1.000 | 1.000 | 1.000 | 1.000 | 1.000 |
| C ⁴⁺ | 1.000 | 1.000 | 1.000 | 1.000 | 1.000 | 1.000 | 1.000 | 1.000 | 1.000 | 1.000 | 1.000 | 1.000 | 1.000 | 1.000 | 1.000 |

calculated empirical formulae are based on sum of Ca + Mn + Sr + Mg + Fe = 6 apfu, CO₂ was calculated based on stoichiometry

from 0.13 to 0.39 apfu) was also detected. Furthermore, minor concentrations of Mg (up to 0.09 apfu) and Fe (up to 0.03 apfu) are also present.

4.4. Other gangue minerals

Quartz predominantly occurs as subhedral to euhedral grains which enclose aggregates of sulfides or are dispersed in a fine-grained mixture of Mn-rich calcite and Mn-silicates, sometimes in association with chlorite or adularia.

Clinzoisite was observed only in the younger black veinlets developed in the calcite part of the vein. It usually forms subhedral grains up to 100 μm in size in association with rhodochrosite in intergranular spaces. Except of Ca and Al, also minor amounts of Mn (up to 0.10 apfu) and Fe (up to 0.09 apfu) were detected.

Clinocllore was rarely found as fibrous aggregates up to 500 μm in association with quartz and intimately intergrown with Mn-rich calcite or fill intergranular spaces between older johannsenite. Elevated contents of Fe (up to 0.60 apfu) as well as minor amounts of Mn (up to 0.02 apfu) were detected in studied samples.

4.5. Ore minerals

All ore minerals occur in cavities of Mn-silicate aggregates, associated with quartz, chlorite, adularia and youngest Mn-calcite.

4.5.1. Sphalerite

Sphalerite is the most common ore mineral in the studied vein. It forms subhedral to anhedral grains and aggregates up to several mm in size (Figs 9a,b), often associated with Mn-rich calcite, quartz, galena as well as rare chalcopryrite and acanthite. Chemical analyses of sphalerite are presented in Tab. 4. It contains a small amount of Fe (up to 0.03 apfu), Mn (up to 0.02 apfu) and Cd (up to 0.004 apfu).

4.5.2. Galena

Galena is the second most common ore mineral after sphalerite. It occurs as anhedral, often rounded grains associated with other ore minerals (Figs 9a,b), especially sphalerite. An average (n=4) empirical formula of galena based on the sum of all atoms = 2 apfu is corresponding to $Pb_{1.00}Fe_{0.02}S_{0.98}$.

4.5.3. Pyrite

Pyrite is less abundant than galena and sphalerite. It usually forms separate, subhedral to anhedral grains

enclosed in fine grained johannsenite–rhodonite mass or in Mn-rich calcite. Pyrite does not contain impurities and its average ($n=6$) empirical formula is $\text{Fe}_{0.99}\text{S}_{2.01}$.

4.5.4. Chalcopyrite

Chalcopyrite occasionally forms coarse-grained aggregates up to 1 cm in size developed on the contact of the vein with the wallrock, where it coexists with sphalerite, galena, and pyrite. More frequently forms anhedral inclusions in sphalerite along with galena (Fig. 9c).

4.5.5. Acanthite

Acanthite was rarely found as rounded inclusions up to 15 μm in size (Figs 9a,d), enclosed together with galena in sphalerite. Quantitative chemical analyses of acanthite are shown in Tab. 4. One analysis shows a minor content of Te (0.02 *apfu*).

4.6. Fluid inclusion study

The study of fluid inclusions was performed on two double-sided polished plates, which represent the johannsenite-rhodonite bearing part of the vein and its contact with the white coarse-grained calcite. Most common were two-phase liquid-vapor inclusions hosted

Tab. 4 Quantitative chemical analyses of sphalerite and acanthite (in wt. %).

| | 1 | 2 | 3 | 4 | 5 | 6 | 7 | 8 | 9 |
|----------|--------|-------|-------|--------|--------|--------|-------|-------|-------|
| | Sp | Sp | Sp | Sp | Sp | Sp | Aca | Aca | Aca |
| Zn | 65.55 | 65.53 | 65.16 | 64.50 | 64.94 | 64.65 | 0.00 | 0.00 | 0.00 |
| Fe | 0.88 | 0.91 | 1.15 | 1.30 | 1.58 | 1.25 | 0.00 | 0.00 | 0.00 |
| Mn | 0.36 | 0.40 | 0.32 | 1.08 | 0.88 | 1.13 | 0.00 | 0.00 | 0.00 |
| Cd | 0.34 | 0.32 | 0.29 | 0.31 | 0.34 | 0.41 | 0.00 | 0.00 | 0.00 |
| Cu | 0.00 | 0.00 | 0.00 | 0.08 | 0.00 | 0.09 | 0.06 | 0.44 | 0.21 |
| Ag | 0.00 | 0.00 | 0.00 | 0.00 | 0.00 | 0.00 | 86.77 | 86.02 | 85.75 |
| As | 0.00 | 0.00 | 0.00 | 0.00 | 0.00 | 0.00 | 0.21 | 0.12 | 0.00 |
| S | 32.98 | 32.73 | 32.65 | 32.84 | 33.31 | 32.82 | 12.77 | 12.28 | 13.10 |
| Se | 0.00 | 0.00 | 0.00 | 0.00 | 0.00 | 0.00 | 0.06 | 0.00 | 0.08 |
| Te | 0.00 | 0.00 | 0.00 | 0.00 | 0.00 | 0.00 | 0.10 | 0.94 | 0.08 |
| total | 100.10 | 99.90 | 99.56 | 100.11 | 101.05 | 100.34 | 99.96 | 99.80 | 99.21 |
| Zn | 0.975 | 0.978 | 0.975 | 0.959 | 0.955 | 0.960 | 0.000 | 0.000 | 0.000 |
| Fe | 0.015 | 0.016 | 0.020 | 0.023 | 0.027 | 0.022 | 0.003 | 0.000 | 0.000 |
| Mn | 0.006 | 0.007 | 0.006 | 0.019 | 0.015 | 0.020 | 0.000 | 0.000 | 0.000 |
| Cd | 0.003 | 0.003 | 0.002 | 0.003 | 0.003 | 0.004 | 0.000 | 0.000 | 0.000 |
| Cu | 0.000 | 0.000 | 0.000 | 0.001 | 0.000 | 0.001 | 0.002 | 0.017 | 0.008 |
| Ag | 0.000 | 0.000 | 0.000 | 0.000 | 0.000 | 0.000 | 1.996 | 2.000 | 1.974 |
| As | 0.000 | 0.000 | 0.000 | 0.000 | 0.000 | 0.000 | 0.007 | 0.004 | 0.000 |
| Σ | 1.000 | 1.004 | 1.004 | 1.005 | 1.001 | 1.006 | 2.008 | 2.021 | 1.982 |
| S | 1.000 | 0.996 | 0.996 | 0.995 | 0.999 | 0.994 | 0.988 | 0.961 | 1.014 |
| Se | 0.000 | 0.000 | 0.000 | 0.000 | 0.000 | 0.000 | 0.002 | 0.000 | 0.002 |
| Te | 0.000 | 0.000 | 0.000 | 0.000 | 0.000 | 0.000 | 0.002 | 0.018 | 0.002 |
| Σ | 1.000 | 0.996 | 0.996 | 0.995 | 0.999 | 0.994 | 0.992 | 0.979 | 1.018 |

calculated empirical formulae are based on sum of all atoms

by johannsenite (Fig. 10a), rhodonite, Mn-rich calcite, sphalerite, and calcite. In the coarse-grained white calcite single-phase vapor-rich inclusions were also observed. They probably represent empty vugs and/or stretched inclusions, however, some of them were found in association with liquid-rich inclusions and with inclusions with various liquid and vapor ratios which is indicative of trapping of a boiling fluid (Fig. 10b). The dimensions of the fluid inclusions ranged from 3 to 55 μm . Mostly primary inclusions were studied, however,

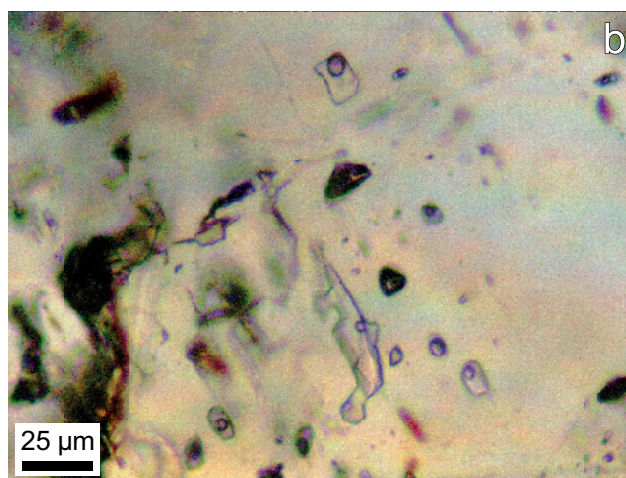
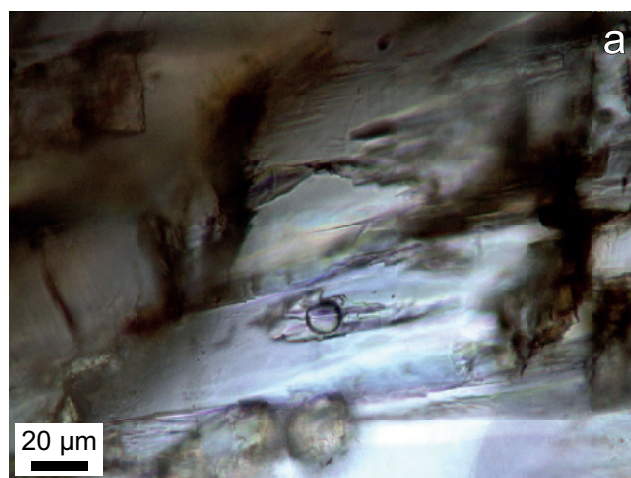


Fig. 10a – Typical two-phase primary liquid-vapor inclusion enclosed in johannsenite. **b** – Vapor-rich inclusions in association with liquid-rich inclusions with various liquid/vapor ratios enclosed in calcite from the white part of the vein.

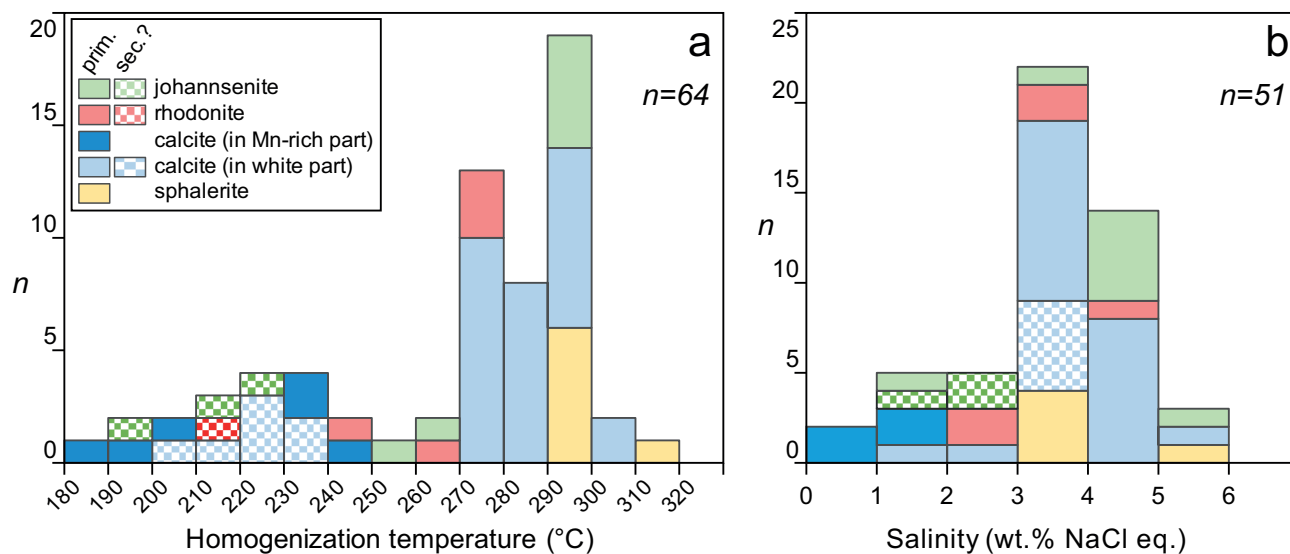


Fig. 11a – Summary histogram of fluid inclusion homogenization temperatures. **b** – Summary histogram of salinities. *n* – number of measurements.

a few secondary inclusions were measured as well. In total, 70 individual fluid inclusions were measured to obtain ice melting (T_m) and homogenization temperatures (T_h ; always to liquid state). Eutectic temperatures (T_e) were observed just in primary fluid inclusions in johannsenite and Mn-rich calcite. The measured T_e ranged between -36.6 and -34.2 °C and may correspond to the system $H_2O-NaCl-MgCl_2$ (Shepherd et al. 1985). However, according to experimental studies of Borisenko (1977), Davis et al. (1990), and Spencer et al. (1990) other chlorides could be also present, especially Fe, or K.

Primary inclusions in johannsenite provided T_h values from 257 to 295 °C. The measured values of T_m correspond to salinities from 3.1 to 5.3 wt. % NaCl eq. Secondary inclusions in johannsenite had T_h intervals ranging from 198 to 222 °C and salinity concentrations from 1.7 to 2.4 wt. % NaCl eq. (Figs 11a,b).

In rhodonite only primary inclusions could be found. Their T_h values are ranged from 214 to 274 °C and salinity from 2.4 to 4.6 wt. % NaCl eq. (Figs 11a,b).

Primary fluid inclusions in Mn-rich calcite from Mn-rich part of vein (from interstitial spaces or cavities in johannsenite–rhodonite aggregates) had T_h values ranging from 187 to 249 °C and salinity from 0.4 to 4.6 wt. % NaCl eq. Calcite from the main mass of the white part of the vein had primary and secondary fluid inclusions. Primary fluid inclusions had T_h values ranging from 208 to 305 °C and salinity from 1.9 to 5.0 wt. % NaCl eq., while secondary fluid inclusions had T_h values from 223 to 232 °C and salinity from 3.1 to 3.5 wt. % NaCl eq. Primary fluid inclusions in sphalerite yielded T_h values ranging from 290 to 318 °C and salinities from 3.2 to 5.1 wt. % NaCl eq. (Figs 11a, b).

5. Discussion

The presence of Mn-bearing silicates and carbonates is one of the typical characteristics of intermediate-sulfidation epithermal deposits and it is a common diagnostic feature to discern them from low sulfidation deposits (Sillitoe and Hedenquist 2003; Wang et al. 2019). Mn silicates, including rare johannsenite, typically appear early in the depositional history of epithermal systems, just before or during the main stage of sulfide deposition. The most common Mn-silicate mineral is rhodonite that is often replaced or accompanied by rhodochrosite, which typically originates in mid to late hydrothermal stages (Marcoux et al. 1993, 1996; Milési et al. 1994, 1999; Cooke et al. 1996; Bailly et al. 1998; Piantone et al. 1999; Wang et al. 2019; Leroy et al. 2000). In agreement with this observation, johannsenite from the Rozália mine is earlier than sulfides and Mn-carbonates, representing paragenetically the oldest mineral in the studied vein.

Johannsenite is a mineral that belongs to the clinopyroxene group and it typically occurs in metasomatized limestones, polymetallic skarns, and in some types of metamorphic Mn-ores (Sugaki et al. 1985; Cabella et al. 1991; Nayak et al. 1997; Capitani and Mellini 2000; Demirela et al. 2010; Han and Choi 2012; Wang et al. 2014; Palinkas et al. 2018). In epithermal systems, johannsenite is less frequently reported, occurring in Au–Ag and Ag–Au±Pb–Zn vein mineralization of intermediate sulfidation type. In these systems, johannsenite is accompanied by rhodonite and calcite (e.g., Tayoltita deposit in Mexico; Smith et al. 1982; Clarke and Titley 1988), rhodochrosite and/or Mn-calcite (e.g., Bunikasih deposit in Western Java; Subandrio and Basuki 2010; and Koryu deposit in Japan; Shimizu et al. 1998) or rhodonite and bustamite (Caylloma district in Peru; Echavarría et

al. 2006). In the studied vein, johannsenite is mostly accompanied by rhodonite and calcite, which best resembles to the johannsenite assemblage from the Tayoltita Ag-Au deposit. Due to the lack of published chemical compositions of johannsenite from epithermal systems, our analytical data can be compared just to johannsenite from the Koryu mine, where it has much higher Fe (up to 2.1 *apfu*) and Mg (up to 0.27 *apfu*) contents (Sugaki et al. 1985) than in studied vein. Interestingly, johannsenite in other types of mineralizations (skarns, metamorphic Mn deposits) usually also have much higher Fe and Mg contents than johannsenite at the Rozália mine (Sijakova-Ivanova and Boev 1997; Schaller 1938).

The studied vein with johannsenite represents a new type of Mn-mineralization at the Rozália mine, but also in the entire area of the Štiavnica stratovolcano. As presented above, according to the structural properties and relative age it belongs to the system of post-caldera Cu-Pb-Zn±Ag-Au veins. However, the occurrence of Mn-mineralization was not known yet at this type of veins at deep levels of the Rozália mine and its presence does not correspond to their typical vertical zonality, as rhodonite and rhodochrosite typically occur just in the upper parts of post-caldera veins, in their upper Pb-Zn zone (Koděra 1955; Jeleň 1988; Kovalenker et al. 1991). Nevertheless, the studied vein with increased Pb+Zn content (1.2 %), and a low Cu content (42 ppm) chemically resembles to the Pb-Zn and not to the Cu zone which typically occurs at deep levels of the Rozália mine. Chemical compositions of rhodonite, sphalerite, carbonates and chlorite are also similar to compositions of these minerals in the Pb-Zn zone (Jeleň 1988). The presence of acanthite and their increased Te content was also observed in other post-caldera veins (up to 1.1 wt. % Te; Chovan et al. 2019).

To our knowledge, fluid inclusion microthermometry on johannsenite was not performed yet on any of the epithermal systems worldwide, however, there exist limited data from accompanying quartz from the same stage as johannsenite from Tayoltita, Koryu and Caylloma deposits (Smith et al. 1982; Shimizu et al. 1998; Echavarría et al. 2006), that provided homogenization temperature ranges 250–290 °C, 263–283 °C and 225–308 °C, respectively. Corresponding

salinity ranges were 3.3–8.4, 0.5–6.0, 0.5–6.6 wt. % NaCl eq., while boiling of fluids was determined in all 3 deposits. These data are very similar to the results obtained from fluid inclusions in the studied vein mineralization (187–318 °C, 0.4–5.3 wt. % NaCl eq.). The histogram of homogenization temperatures (Fig. 11a) shows that two main stages of fluid evolution were participating on the studied mineralization. The higher temperature range stage (~270–300 °C) corresponds to the crystallization of johannsenite, rhodonite, sphalerite and main mass of calcite, followed by precipitation of rhodonite at the lower end of this Th range. During the lower temperature range (~210–240 °C), Mn-rich calcite has crystallized in cavities in Mn-silicate aggregates and calcite aggregates, probably temporally associated with the origin of clinozoisite-rhodochrosite veinlets. The data show a trend of simultaneous decrease in salinity and homogenization temperatures, indicative of mixing of fluids of different salinity and temperature, probably magmatic and meteoric in origin (Fig. 12). Compared to the published microthermometric data from the post-caldera base metal veins, located eastward of the Rozália mine (Th 100–380 °C, 0.5–11.5 wt. % NaCl eq.; Kovalenker et al. 1991), they show a clear overlap including the trend of mixing of magmatic and meteoric fluids.

As discussed above, johannsenite and calcite have probably precipitated nearly simultaneously in different parts of the vein, which is supported by their similar microthermometric data. However, only in calcite it was determined boiling of fluids, but it is likely that fluid related to Mn-silicates was also affected by this phenomenon as seen on other epithermal deposits with johannsenite. This is indicated by the fact that the solubility of rhodonite is retrograde, and it cannot precipitate during a simple episode of cooling. According to Gammons and Seward (1996), its precipitation is caused by a sudden increase

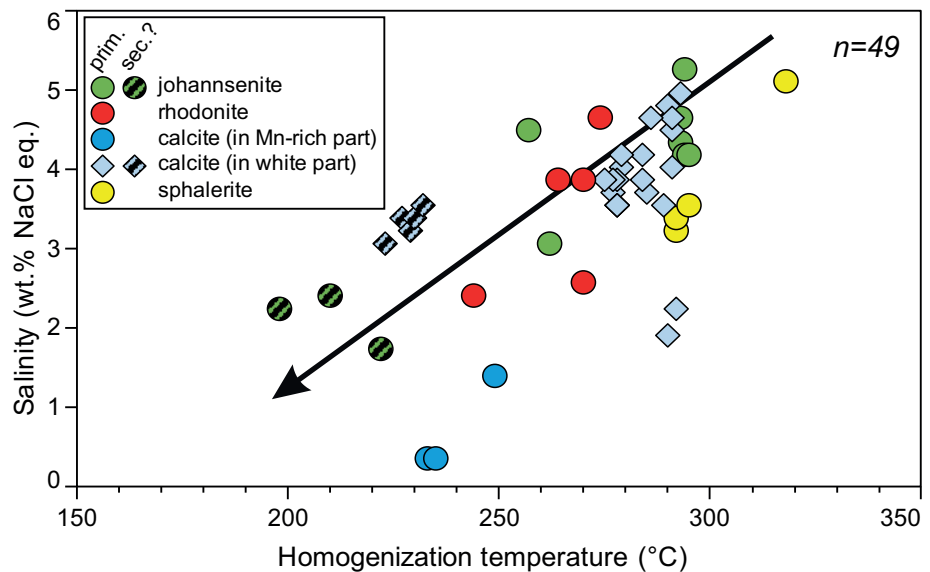


Fig. 12 Diagram of salinity vs. homogenization temperatures in fluid inclusions for all studied minerals. *n* – number of measurements.

in pH due to fluid boiling or a decrease in chloride concentration due to fluid dilution (Leroy et al. 2000) which is also apparent from our fluid inclusion data.

Boiling of fluids enables to calculate fluid pressure and paleodepth of formation of the mineralization. Based on minimum homogenisation temperatures of primary fluid inclusions in calcite boiling of fluids with salinity of 3.5 to 4.2 wt. % NaCl eq. occurred from 275 to 279 °C and fluid pressures, modelled in the system H₂O–NaCl (Haas 1971, 1976), range from 58 to 62 bars. The calculated minimum depths, assuming no effect from dissolved CO₂ and hydrostatic pressure conditions, range from 704 to 752 m. This agrees with the depth of 600–700 m calculated by Kovalenker et al. (1991) from fluid inclusions from stage 4 of the post-caldera Terézia vein, sampled from a similar depth (240 and 95 m a.s.l.) as the studied vein. Similar paleodepths (780±60 m) were also obtained from the 4th stage of the Rozália vein at the 14th level of the Rozália mine (240 m a.s.l.; Koděra et al. 2005). However, historical fluid inclusion data from the 3rd stage of the post-caldera veins, that frequently contain Mn-minerals on upper parts of the veins, are not available.

6. Conclusions

The newly discovered type of Mn-rich vein mineralization at the Rozália mine represents a new type of Mn-mineralization in the entire area of the Štiavnica stratovolcano. It belongs to the system of post-caldera veins, related to the resurgent horst-uplift during the late-stage of evolution of the Štiavnica stratovolcano. It is of intermediate sulfidation type, and consists of abundant johannsenite, rhodonite and calcite, accompanied by minor chlorite, quartz, adularia, rare ore minerals (pyrite, sphalerite, galena, chalcopyrite and acanthite) and late Mn-carbonates (rhodochrosite, Mn-rich calcite) and clinzoisite. The presence of Mn-mineralization at the 18th level of the Rozália mine does not correspond to the typical vertical zonality of post-caldera veins, where abundant Mn-minerals are known just from higher levels of the veins in their Pb–Zn zone. However chemically, with its high Pb+Zn/Cu ratio, the vein is similar to this zone.

Fluid inclusion microthermometry confirms the observed paragenetical relationships in the vein, as johannsenite, rhodonite, sphalerite and calcite have crystallised at significantly higher temperature than later Mn-rich calcite. Precipitation of calcite, and probably also Mn-silicates, was triggered by fluid boiling, later accompanied by mixing of fluids probably of magmatic and meteoric origin. The obtained fluid properties (187–318 °C, 0.4–5.3 wt. % NaCl eq.) are similar to fluids of other post-caldera veins in the vicinity of the Rozália

mine in similar depth, including the observed boiling and fluid mixing trend, and the similar calculated paleodepth of boiling (from 704 to 752 m). To our knowledge, this the first direct observation of fluid properties related to crystallisation of johannsenite in epithermal systems, thus this work contributes to the understanding of genesis of this rare mineral in epithermal environment worldwide.

Acknowledgements. This study was supported by grants of the Slovak Research and Development Agency (contracts No. APVV-15-0083 and APVV-0033-07), Research Agency of the Ministry of Education, Science, Research and Sport of the Slovak Republic (contracts No. VEGA 1/0313/20 and VEGA 2/0029/23), Comenius University (contract No. UK/104/2021), and ERDF (ITMS 262402200). Support by Slovenská Banská, Ltd. is also acknowledged.

References

- BAILLY L, MILÉSI JP, LEROY JL, MARCOUX E (1998) Les minéralisations épithermales à Au–Cu–Zn–Sb du district de Baia Mare (Nord Roumanie). Nouvelles données minéralogiques et microthermométriques. *C R Acad Sci* 327(6), Ser II: 385–390 (in French)
- BODNAR RJ (1993) Revised equation and table for determining the freezing point depression of H₂O–NaCl solutions. *Geochim Cosmochim Acta* 57: 683–684
- BORISENKO AS (1977) Study of salt composition of fluid inclusions in minerals using cryometric technique. *Geol Geofiz* 8: 16–27
- CABELLA R, GAGGERO L, LUCCHETTI G (1991) Isothermal-isobaric mineral equilibria in braunite-, rhodonite-, johannsenite-, calcite-bearing assemblages from Northern Apennine metacherts (Italy). *Lithos* 27: 149–154
- CAMPRUBÍ A, ALBINSON T (2007) Epithermal deposits in Mexico – update of current knowledge, and an empirical reclassification. *Geol Soc Am Special Papers*, pp 1–422
- CAPITANI GC, MELLINI M (2000) The johannsenite-hedenbergite complete solid solution: Clinopyroxenes from the Campiglia Marittima skarn. *Eur J Mineral* 12(6): 1215–1227
- CLARKE M, TITLEY SR (1988) Hydrothermal evolution in the formation of silver-gold veins in the Tayoltita Mine, San Dimas District. *Econ Geol* 83(8): 1830–1840
- COOKE DR, MCPHAIL DC, BLOOM MS (1996) Epithermal gold mineralization, Acupan, Baguio District, Philippines: geology, mineralization, alteration, and the thermochemical environment of ore deposition. *Econ Geol* 91: 243–272
- DAVIS DW, LOWENSTEIN TK, SPENCER RJ (1990) Melting behavior of fluid inclusions in laboratory-grown halite crystals in the system NaCl–H₂O, NaCl–KCl–H₂O,

- NaCl–MgCl₂–H₂O and NaCl–CaCl₂–H₂O. *Geochim Cosmochim Acta* 54: 591–601
- DEMIRELA G, AKISKA S, SAYILI IS, KUŞCU I (2010) Silicate and sulfide mineral chemistry of some carbonate-related Pb–Zn–Cu mineralizations and their effects on ore genesis in NW Anatolia, Turkey. Conference: XIX Congress of the Carpathian Balkan Geological Association At: Thessaloniki, Greece Volume: Geol Balc (Abstract Volume)
- ECHAVARRIA L, NELSON E, HUMPHREY J, CHAVEZ J, ESCOBEDO L, IRIONDO A (2006) Geologic evolution of the Caylloma epithermal vein district, Southern Perú. *Econ Geol* 101: 843–863
- GAMMONS CH, SEWARD TH (1996) Stability of manganese (II) chloride complexes from 25 to 300 °C. *Geochim Cosmochim Acta* 60: 4295–4311
- HAAS JL (1971) The effect of salinity on the maximum thermal gradient of a hydrothermal system at hydrostatic pressure. *Econ Geol* 66: 940–946
- HAAS JL (1976) Physical properties of the coexisting phases and thermochemical properties of the H₂O component in boiling NaCl solutions. *Bull US Geol Surv* 1421-A: 1–73
- HAN JK, CHOI SH (2012) Ore Geology of Skarn Ore Bodies in the Kasihan Area, East Java, Indonesia. *Econ Environ Geol* 45(1): 1–8
- HUANG E, CHEN CH, HUANG T, LIN EH, XU JI-AN (2000) Raman spectroscopic characteristics of Mg–Fe–Ca pyroxenes. *Amer Miner* 85: 473–479
- CHOVAN M, KUBAČ A, MIKUŠ T, ŽITNAŇ P, PRCÚCH J (2019) Au–Ag tellurides and sulphosalts from epithermal Au–Ag–Pb–Zn–Cu deposit Banská Hodruša at the Rozália mine (Slovakia). *AGEOS* 11(2): 43–62
- JELEŇ S (1988) Mineral assemblages and formation conditions of ores in the Banská Štiavnica. PhD dissertation, GÚSAV, Banská Bystrica: 247 (in Russian)
- JELEŇ S, PRŠEJ J, KOVALENKER VA, TOPA D, SEJKORA J, ŠTEVKO M, OZDÍN D (2012) Bismuth sulfosalts of the cuprobismutite, pavonite and aikinite series from the Rozália mine, Hodruša–Hámre, Slovakia. *Canad Mineral* 50: 325–340
- KODĚRA M (1955) Rodonit z Banskej Štiavnice. *Geol Sbor Slov Akad Vied (Bratislava)* 6(3–4): 227–231
- KODĚRA M (1963) Gesetzmässigkeiten der zonalen Verteilung der Mineralisation an der subvulkanischen polymetallischen Lagerstätte Banská Štiavnica. In Symposium: Problems of Postmagmatic ore Deposition, Prague, Ústřední ústav geol 1: 227–231
- KODĚRA P, LEXA J, RANKIN AH, FALICK AE (2004) Fluid evolution in a subvolcanic granodiorite pluton related to Fe and Pb–Zn mineralization, Banská Štiavnica ore district, Slovakia. *Econ Geol* 99: 1745–1770
- KODĚRA P, LEXA J, RANKIN AH (2005) Epithermal gold veins in a caldera setting: Banská Hodruša, Slovakia. *Miner Depos* 39: 921–943
- KONEČNÝ V, LEXA J, HOJSTRIČOVÁ V (1995) The Central Slovakia Neogene Volcanic Field: a review. *Acta Vulcanol* 7: 63–78
- KOVALENKER VA, JELEŇ S, LEVIN KA, NAUMOV VB, PROKOFJEV VJ, RUSINOV VL (1991) Mineral assemblages and physical-chemical model of the formation of gold-silver-polymetallic mineralisation on the deposit Banská Štiavnica (Central Slovakia). *Geol Carpath* 42: 291–302
- KUBAČ A, CHOVAN M, KODĚRA P, KYLE JR, ŽITNAŇ P, LEXA J, VOJTKO R (2018) Mineralogy of the epithermal precious and base metal deposit Banská Hodruša at the Rozália mine (Slovakia). *Mineral Petrol* 112: 705–731
- LEROY JL, HUBÉ D, MARCOUX E (2000) Episodic deposition of Mn minerals in cockade breccia structures in three low-sulfidation epithermal deposits: a mineral stratigraphy and fluid-inclusions approach. *Canad Mineral* 38: 1125–1136
- LEXA J, ŠTOHL J, KONEČNÝ V (1999) Banská Štiavnica ore district: relationship among metallogenetic processes and geological evolution of a stratovolcano. *Miner Depos* 34: 639–665
- MAKRESKI P, JAVANOVSKI G, GAJOVIĆ A, BILJAN T, ANGELOVSKI D, JAĆIMOVIĆ R (2005) Minerals from Macedonia. XVI. Vibrational spectra of some common appearing pyroxenes and pyroxenoids. *J Mol Struct* 788: 102–144
- MARCOUX E, MILÉSI JP, SOHEARTO S, RINAWAN R (1993) Noteworthy mineralogy of Au–Ag–W–Sn (Bi) epithermal deposit of Cirotan, western Java, Indonesia. *Canad Mineral* 31: 727–744
- MARCOUX E, MILÉSI JP, SITORUS T, SIMANDJUNTAK M (1996) The epithermal Au–Ag–(Mn) deposit of Pongkor (West Java, Indonesia). *Indones min J* 2: 1–17
- MERNAGH TP, HOATSON DM (1997) Raman Spectroscopic Study of Pyroxene Structures from the Munnii Munnii Layered Intrusion, Western Australia. *J Raman Spectrosc* 28: 647–658
- MILÉSI JP, MARCOUX E, NEHLIG P, SUNARYA Y, SUKANDAR A, FELENC J (1994) Cirotan, west Java, Indonesia: a 1.7 Ma hybrid epithermal Au–Sn–W deposit. *Econ Geol* 89: 227–245
- MILÉSI JP, MARCOUX E, SITORUS T, SIMANDJUNTAK M, LEROY JL, BAILLY L (1999) Pongkor (west Java, Indonesia): a Pliocene supergene-enriched epithermal Au–Ag–(Mn) deposit. *Miner Depos* 34: 131–149
- NAYAK B, MOHAPATRA BK, SAHOO RK (1997) Mn-pyroxenes from Gangpur Group of rocks, Goriajhar, Orissa, India. *J Miner Petrol Econ Geol* 92(10): 425–430
- PALINKAS SS, PELTEKOVSKI Z, TASEV G, SERAFIMOVSKI T, ŠMAJGL D, RAJIČ K, SPANGENBERG JE, NEUFELD K, PALINKAŠ LA (2018) The Role of Magmatic and Hydrothermal Fluids in the Formation of the Sasa Pb–Zn–Ag Skarn Deposit, Republic of Macedonia. *Geosci (Switz)* 8(12): 444

- PIANTONE P, GRANCEA L, LEROY JL, BAILLY L, MARIAS Z, NEHLING P, MARCOUX E (1999) Fluid inclusion and isotope study of the Cavnic epithermal deposit (Romania). In: STANLEY C.J. ET AL. (eds, deposit.) *Mineral Deposits: Processes to Processing*. A. A. Balkema Publ., Rotterdam, The Netherlands: pp 79–82
- REYES RM, BELTRÁN JMV, JAÍMES MEV, SPURGEON PJ (2016) San Martín de Bolaños, Jalisco, Mexico, NI 43-101 Technical Report on Mineral Resource and Mineral Reserve Update
- SCHALLER WT (1938) Johannsenite, a new manganese pyroxene. *Amer Miner* 23: 575–582
- SEJKORA R, ŠTEVKO M, OZDÍN D, JELEŇ S, PRŠEK J (2015) Unusual morphological forms of hodrušite from the Rozália vein, Hodruša-Hámre near Banská Štiavnica (Slovak Republic). *J Geosci* 60: 11–22
- SHCHIPALKINA NV, PEKOV IJ, CHUKANOV NM, BIAGIONI C, PASERO M (2019) Crystal chemistry and nomenclature of rhodonite-group minerals. *Mineral Mag* 83: 829–835
- SHCHIPALKINA NV, PEKOV IV, CHUKANOV NV, ZUBKOVA NV, BELAKOVSKIY DI, BRITVIN S, KOSHYAKOVA NN (2020) Vittinkiite, $MnMn_4[Si_5O_{15}]$, a member of the rhodonite group with a long history: definition as a mineral species. *Mineral Mag* 84(6): 1–30
- SHEPHERD TJ, RANKIN AH, ALDERTON DHM (1985) A practical guide to fluid inclusion studies. Glasgow, Blackie: pp 1–239
- SHIMIZU T, MATSEUDA H, ISHIYAMA D, MATSUBAYA O (1998) Genesis of epithermal Au–Ag mineralization of the Koryu Mine, Hokkaido, Japan. *Econ Geol* 93: 303–325
- SIJAKOVA-IVANOVA T, BOEV B (1997) Mineralogical characteristics of johannsenite in the Sasa ore field. *Geol Maced* 11: 45–49
- SILLITOE RH, HEDENQUIST JW (2003) Linkages between volcanotectonic settings, ore fluid compositions, and epithermal precious metal deposits. *Soc Econ Geol Special Publication* 10: 315–343
- SIMMONS SF, WHITE NC, JOHN DA (2005) Geological characteristics of epithermal precious and base metal deposits. *Econ Geol 100th Anniversary Volume*, 485–522
- SMITH DM, ALBINSON T, SAWKINS FJ (1982) Geologic and fluid inclusion studies of the Tayoltita silver-gold vein deposit, Durango, Mexico. *Econ Geol* 77: 1120–1145
- SPENCER RJ, MÖLLER N, WEARE JH (1990) The prediction of mineral solubilities in natural waters: a chemical equilibrium model for the Na–K–Ca–Mg–Cl–SO₄–H₂O systems at the temperatures below 25 °C. *Geochim Cosmochim Acta* 54: 575–590
- SUBANDRIO AS, BASUKI NI (2010) Alteration and vein textures associated with gold mineralization at the Bunikasih Area, Pangalengan, West Java. *Indones J Geosci* 5(4): 247–261
- SUGAKI A, KITAZAKE A, ISOBE K (1985) Johannsenite from the Koryu mine, Hokkaido, Japan. *Mineral J* 12: 341–348
- ŠTOHL J, LEXA J, KALIČIAK M, BACSÓ Z (1994) Metalogenéza žilníkových polymetalických mineralizácií v neovulkanitoch Západných Karpát. *Miner Slov* 26: 75–117
- WANG BG, QIN KZ, SONG GX, LI GM (2019) A review of intermediate sulfidation epithermal deposits and subclassification. *Ore Geol Rev* 107: 434–456
- WANG LQ, TANG JX, CHEN W, LUO MC, KANG HR, LENG QF (2014) Mineralogical characteristics of skarn in the Bangpu Mo polymetallic deposit, Tibet, and their geological significance. *Geol China* 41(2): 562–576